ANTIOXIDANTS & REDOX SIGNALING
Volume 11, Number 6, 2009

DOI: 10.1089/ars.2008.2407

Forum Original Research Communication

Endosomal Nox2 Facilitates Redox-Dependent Induction of NF-κB by TNF-α

Qiang Li,[1] Netanya Y. Spencer,[1,2] Fredrick D. Oakley,[1,3] Garry R. Buettner,[5] and John F. Engelhardt[1,2,4]

Abstract

Growing evidence suggests that NADPH oxidase (Nox)-derived reactive oxygen species (ROS) play important roles in regulating cytokine signaling. We have explored how TNF-α induction of Nox-dependent ROS influences NF-κB activation. Cellular stimulation by TNF-α induced NADPH-dependent superoxide production in the endosomal compartment, and this ROS was required for IKK-mediated activation of NF-κB. Inhibiting endocytosis reduced the ability of TNF-α to induce both NADPH-dependent endosomal superoxide and NF-κB, supporting the notion that redox-dependent signaling of the receptor occurs in the endosome. Molecular analyses demonstrated that endosomal H_2O_2 was critical for the recruitment of TRAF2 to the TNFR1/TRADD complex after endocytosis. Studies using both Nox2 siRNA and Nox2-knockout primary fibroblasts indicated that Nox2 was critical for TNF-α–mediated induction of endosomal superoxide. Redox-active endosomes that form after TNF-α or IL-1β induction recruit several common proteins (Rac1, Nox2, $p67^{phox}$, SOD1), while also retaining specificity for ligand-activated receptor effectors. Our studies suggest that TNF-α and IL-1β signaling pathways both can use Nox2 to facilitate redox activation of their respective receptors at the endosomal level by promoting the redox-dependent recruitment of TRAFs. These studies help to explain how cellular compartmentalization of redox signals can be used to direct receptor activation from the plasma membrane. *Antioxid. Redox Signal.* 11, 1249–1263.

Introduction

Redox regulation has been shown to be critical in a number of physiologic and pathologic processes, such as cancer, diabetes, and cardiovascular diseases (21, 62). In this context, reactive oxygen species (ROS), such as $O_2^{\bullet-}$ and H_2O_2, have been shown to be induced in cells after receptor stimulation with various ligands such as tumor necrosis factor alpha (TNF-α) (12, 39), lipopolysaccharide (LPS) (24, 51), angiotensin II (18), platelet-derived growth factor (PDGF) (56), insulin (37), epidermal growth factor (EGF) (2), and interleukin-1β (IL-1β) (6, 39). Furthermore, the induction of ROS by these ligands has been suggested to be important for activating many of these signaling pathways (2, 18, 33, 56). These findings suggest that a variety of signaling pathways are mediated by ROS.

Considering the diffusibility of ROS and the high concentrations of redox-reactive biomolecules in the cytoplasm, the mechanism by which ROS facilitate specific signals has been increasingly studied during recent years. Current evidence suggests that significant control of ROS signals are imparted by spatially restricted production at intracellular sites where redox-regulated signaling occurs. For example, NADPH oxidases are recognized to control spatially the production of ROS during cell signaling (59). Seven known NADPH oxidase catalytic subunits exist, which share similar mechanisms of generating superoxide ($O_2^{\bullet-}$) by transferring an electron from NADPH to molecular oxygen (Nox1, $Nox2^{gp91phox}$, Nox3, Nox4, Nox5, Duox1, Duox2) (29). Among these Nox isoforms, the phagocytic Nox2 ($gp91^{phox}$) is the most widely characterized NADPH oxidase and has also been found to be expressed in a variety of nonphagocytic cell types (18, 32, 47). Activation

[1]Department of Anatomy and Cell Biology, [2]Department of Internal Medicine, [3]Medical Scientist Training Program, and the [4]Center for Gene Therapy, [5]Free Radical and Radiation Biology Program, Department of Radiation Oncology, Carver College of Medicine, The University of Iowa, Iowa City, Iowa.

of the Nox2 complex requires association of several proteins at the membrane, including $p67^{phox}$, $p47^{phox}$, and $p22^{phox}$; Rac1/2, a small GTPase, also plays an important role in activating $O_2^{\bullet-}$ production by this complex (29).

Nox proteins have been increasingly recognized as key elements of intracellular signaling. For example, Nox2 has been demonstrated to produce endosomal $O_2^{\bullet-}$ required for IL-1β induction of NF-κB (32). Expression of a dominant-negative Nox4 or Nox4-siRNA attenuates insulin-stimulated H_2O_2 production and downstream phosphatase signaling involved in adipocyte insulin-receptor activation (37). TNF-α also has been hypothesized to use Nox2-dependent production in its activation cascades (1). Supportive evidence includes the demonstration that inhibition of Rac1 or $p47^{phox}$ abrogates TNF-α–stimulated H_2O_2 production and NF-κB activation (12, 15, 31). Additionally, Nox1 has been associated with ROS producing endosomes required for IL-1β or TNF-α induction of NF-κB in vascular smooth muscle cells (41). Despite the clear association of Nox proteins with redox signaling, the redox-dependent events that control many of these activation pathways remain largely unknown.

The present study seeks to clarify redox-dependent components of TNF-α signaling that are important for NF-κB activation. NF-κB, a ubiquitous transcription factor, has been shown to mediate the expression of genes responsible for the activation of immune and inflammatory responses (17). TNF-α is one of the most broadly studied cytokines known to activate NF-κB (3). The signal from TNF-α is mediated by two cell-surface receptors, TNFR1 and TNFR2 (38, 57). The binding of TNF-α triggers receptor activation, resulting in the recruitment of a number of cytoplasmic signaling proteins to the TNFR complex. For example, TRAF2 interacts directly with TNFR2 (50), but it is recruited to TNFR1 *via* its interaction with TNFR1-associated death-domain protein (TRADD) (22, 23). TRAF2 is a member of the TRAF protein family that includes six members (TRAF1-6) (10, 25) that generally act as adaptor proteins. TRAF2 and RIP recruitment to TNFR1/TRADD complexes is required for the activation of the IKK complex and NF-κB (30).

In the present study, we investigated the redox-dependent events responsible for TNF-α/TNFR1–mediated NF-κB activation. The focus of these studies was to determine how TNFR1 activation of the IKK complex is coordinated by Nox-derived ROS. In contrast to current thinking (30), we observed that a significant portion of TNF-α–mediated NF-κB activation requires endocytosis of the receptor. Endocytosis was essential for the activation of Nox2-dependent endosomal ROS required for TRAF2 recruitment to the TNFR1/TRADD complex and the activation of IKK and NF-κB. In contrast, TRADD efficiently recruited to TNF/TNFR1 at the plasma membrane in the absence of endocytosis. The recruitment of TRAF2 to the TNFR1/TRADD complex could be partially reconstituted at the plasma membrane in the absence of endocytosis by the addition of exogenous H_2O_2, suggesting that Nox2 is a source of endosomal H_2O_2 required for TNFR1 activation. Clearance of ROS from the endosomal compartment also significantly reduced both IKK and NF-κB activation after TNF-α stimulation. Through this process, the generation of $O_2^{\bullet-}$ by endosomal Nox2, and its conversion to H_2O_2, facilitates the redox-dependent formation of an active TNFR1 complex required for redox-dependent NF-κB activation. This mechanism helps clarify how cells can partition Nox-derived ROS to selectively influence receptor activation from the plasma membrane.

Materials and Methods

Recombinant expression vectors and small interfering RNA (siRNA)

MCF-7 cells were infected with recombinant adenoviruses (500 particles per cell) as previously described (33); cells were used for experiments at 48 h after infection. The following E1-deleted recombinant adenoviral vectors were used: (a) Ad.GPx-1, which encodes glutathione peroxidase 1 and degrades cytoplasmic H_2O_2 (33); (b) Ad.Dyn(DN), which encodes a dominant-negative mutant (K44A) of dynamin and inhibits endocytosis (13); (c) Ad.NF-κBLuc, which encodes an NF-κB–responsive promoter driving luciferase expression and was used to assess NF-κB transcriptional activation *in vivo* (51); and (d) Ad.BglII, an empty vector with no insert, as a control for viral infection (33). For NF-κB transcriptional assays using infection with two recombinant adenoviruses, a slightly modified sequential infection method was used (51). In this case, cells were infected with experimental vectors [*i.e.*, Ad.Dyn(DN) or Ad.GPx1] 24 h before infection with Ad.NF-κBLuc], and cells were used for experiments at 48 h after initial infection. Transduction efficiencies with recombinant adenoviruses were typically 80–90%, as assessed by Ad.CMV-GFP reporter gene expression. siRNAs against Nox2 (32) were obtained from Santa Cruz Biotechnology (Santa Cruz, CA); transfections were performed by using methods and reagents described by the manufacturer. The sequences used for the siRNAs were proprietary and were not provided by the company.

Cytokine treatments and vesicular isolation

MCF-7 cells were treated with recombinant TNF-α (0.5 ng/ml) or IL-1β (1 ng/ml) for 20 min before vesicular isolation, whereas primary mouse dermal fibroblasts were treated with 10 ng/ml TNF-α. For antioxidant enzyme endosomal loading experiments, purified bovine Cu/Zn superoxide dismutase (SOD1; Oxis Research, Foster City, CA) or catalase (Sigma-Aldrich, St. Louis, MO) proteins or both were diluted from concentrated stocks in PBS into fresh medium to a final concentration of 1 mg/ml and then applied to cells 10 min before cytokine treatment in the continued presence of SOD or catalase or both. Cells were washed and scraped into ice-cold phosphate-buffered saline (PBS). Cell pellets were then resuspended in 0.5 ml of homogenization buffer (0.25 *M* sucrose, 10 m*M* triethanolamine, 1 m*M* EDTA, 1 m*M* phenylmethylsulfonyl fluoride, and 100 μg/ml aprotinin), homogenized in a Duall tissue grinder, and centrifuged at 2,000 *g* at 4°C for 10 min. The supernatant was designated the postnuclear supernatant (PNS). The PNS was subsequently combined with a 60% Iodixanol (OptiPrep Axis-Shield, Norton, MA) solution to obtain a final concentration of 32% and then bottom loaded into an SW55Ti centrifuge tube under two-step gradients of 24% and 20% Iodixanol in homogenization buffer. Samples were centrifuged at 88,195 *g* for 2 h at 4°C. Fractions were collected from the top to the bottom of the centrifuge tube at 4°C (300 μl per fraction) and used immediately for NADPH oxidase activity and immunoisolation assays or were frozen for Western blot assays.

NF-κB and NADPH oxidase activity assays

NF-κB transcriptional activity was assessed by using the previously described NF-κB–inducible luciferase reporter vector (Ad.NF-κBLuc) (51). Luciferase activity was assessed at 6 h after cytokine treatment (unless otherwise specified) by using 5 μg of cell lysate. NADPH oxidase activities were analyzed by measuring the rate of O_2^- generation with a chemiluminescent, lucigenin-based assay (35), as previously applied to vesicles (32). In brief, 5 μ*M* lucigenin (Sigma-Aldrich) in PBS was incubated with vesicular fractions for 10 min in the dark, and reactions were initiated by addition of 100 μ*M* NADPH (Sigma-Aldrich). The change in luminescence was then measured over the course of 3 min (five readings per second).

Vesicular immunoisolation

Rac1-containing endosomes were isolated based on a previous method (58). Cells were infected with Ad.HA-Rac1 48 h before TNF-α treatment. After Iodixanol isolation of intracellular vesicles, one-half of the combined peak vesicular fraction was used directly for biochemical analyses, and the other half was used for immunoaffinity isolation by using Dynabeads M-500 (Dynal Bioscience, Oslo, Norway) coated with the anti-HA antibody. Before use, beads were coated with antibodies as follows: the secondary antibody (anti-rat antibody) was conjugated to Dynabeads (4×10^8 beads/mL) in 0.1 *M* borate buffer (pH 9.5) for 24 h at 25°C with slow rocking. The beads were then placed into the magnet for 5 min and washed in 0.1% (wt/vol) bovine serum albumin (BSA)-PBS for 5 min at 4°C. A final wash in 0.2 *M* Tris (pH 8.5)-BSA was performed for 24 h. Finally, the beads were resuspended in BSA-PBS and conjugated to 4 μg of primary anti-HA antibody per 10^7 beads overnight at 4°C and then washed in BSA-PBS. Vesicular fractions were mixed with 700 μl of coated beads in PBS containing 2 m*M* EDTA, 5% BSA, and protease inhibitors. The mixture was incubated for 6 h at 4°C with slow rocking, followed by magnetic capture and washing in the same tube 3 times (15 min each). Beads with HA-enriched endosomes were then resuspended in PBS, and wash supernatants were saved for analysis.

Western blotting, immunoprecipitations, and in vitro *kinase assays*

Western blotting was performed by using standard protocols, and protein concentrations were determined by using the Bio-Rad protein quantification kit. Immunoreactive proteins were detected by using enhanced chemiluminescence (ECL; GE Healthcare, Piscataway, NJ) or an Odyssey Infrared Imaging System (LI-COR Biotech, Lincoln, NE). Antibodies used for Western blotting were as follows: anti-HA, anti-Rab5, and anti-Rac1 antibodies (BD Transduction Laboratories, Lexington, KY); anti-$p67^{phox}$, anti-TRAF2, anti-TRAF6, anti-IKK, anti-TRADD, anti-TNFR1, anti-IL-1R1, and anti-glutathione *S*-transferase (anti-GST) antibodies (Santa Cruz Biotech); and anti-Cu/ZnSOD antibody (Binding Site, Inc., San Diego, CA).

For immunoprecipitations, cells were washed with ice-cold PBS and lysed in radioimmunoprecipitation assay (RIPA) buffer at 4°C for 30 min. A 500-μg aliquot of cellular protein and 5 μl of primary antibody were mixed with 1 ml of RIPA buffer at 4°C for 1 h. A 50-μl volume of protein A-agarose beads (Santa Cruz Biotech) was then added to the mixture and rotated for 4 h. The beads were washed with ice-cold PBS before experimental analyses.

In vitro kinase assays were performed with immunoprecipitated IKK by using GST-IκBα as a substrate. Kinase reactions were performed with 1 μg GST-IκBα, 0.3 m*M* cold ATP, and 10 μCi [γ-^{32}P]ATP in 10 μl kinase buffer (40 m*M* HEPES, 1 m*M* β-glycerophosphate, 1 m*M* nitrophenolphosphate, 1 m*M* Na_3VO_4, 10 m*M* $MgCl_2$, and 2 m*M* dithiothreitol). The reaction mixtures were then incubated at 30°C for 30 min. Reactions were terminated by the addition of sodium dodecylsulfate–polyacrylamide gel electrophoresis (SDS-PAGE) protein-loading buffer and heated at 98°C for 5 min. After SDS-PAGE, gels were transferred to nitrocellulose membranes and exposed to x-ray film before probing with an anti-GST antibody.

In vivo *localization of endosomal ROS production*

In vivo localization of $O_2^{\bullet-}$ within endosomes was performed by using OxyBURST Green dihydro-2′,4,5,6,7,7′-hexafluorofluorescein (H_2HFF)-BSA (Molecular Probes, Carlsbad, CA). Stock solutions (1 mg/ml) were generated immediately before use by dissolving H_2HFF-BSA in PBS under nitrogen and protected from light. Cells were incubated in the presence of 50 μg/ml OxyBurst Green H_2HFF-BSA for 2 min at 37°C and then stimulated by the addition of TNF-α (0.5 ng/ml). Cells were washed with PBS and fixed in 4% paraformaldehyde for 10 min. After the fixation, cells were mounted in 4′,6′-diamidino-2-phenylindole (DAPI) containing antifadent and examined with fluorescent microscopy.

Generation of Nox-deficient primary dermal fibroblasts

$Nox2^{gp91phox}$-knockout mice (48) were obtained from Jackson Laboratories (strain name: B6.129S6-*Cybbtm1Din*/J; stock number: 002365) and were inbred on the C57BL/6 background. Primary dermal fibroblasts were generated from 1-day-old pups from control C57BL/6 or $Nox2^{gp91phox}$-knockout mice, as previously described (42).

Calculations of endosomal loss during isolation procedures

MCF-7 cells were incubated with Biotin-Transferrin (5 μg/ml) at 37°C for 15 min. Cells were then removed from the plates with trypsin treatment for 5 min, and then carefully washed with cold PBS 3 times. Cell pellets were used to generate PNS for endosomal isolations on Iodixanol gradients, as described earlier. An equal percentage of the PNS and combined Iodixanol endosomal fractions (two through four) were loaded onto an SDS-PAGE for Western blotting with a streptavidin-conjugated 800-nm infrared dye (LI-COR Biotech). Three independent samples were evaluated in this manner, and percentage loss of endosomes during isolation was calculated [100% − (total biotin in the endosomal fraction/total biotin in the PNS)] after quantitative imaging of the Western blots on an Odyssey Infrared Imaging System from LI-COR.

Estimates of $O_2^{\bullet-}$ producing capacity by TNF-α–stimulated redox-active endosomes

Electron paramagnetic resonance spectroscopy (EPR) was used to estimate the capacity of isolated redox-active

endosomes to produce NADPH-dependent $O_2^{\bullet -}$. This method was previously used to specifically detect production of $O_2^{\bullet -}$ by isolated endosomes, which is sensitive to SOD1 but not catalase addition (32). Endosomal fractions were isolated from control (unstimulated) and TNF-α–stimulated MCF7 cells, as described earlier. The isolated endosomal fractions were mixed with 100 μ*M* diethylenetriaminepentaacetic acid (DTPA) and 50 m*M* 5,5-dimethyl-1-pyrroline *N*-oxide (DMPO), in a total volume of 475 μl. The reaction was initiated by adding 25 μl NADPH to a final concentration of 100 μ*M* and then incubated at 37°C for 10 min. Following this incubation period, each sample was immediately placed into the EPR spectrometer and scanned for ~5 min at room temperature. EPR was performed using a Bruker EPR spectrometer in The University of Iowa ESR Core Facility. EPR parameters were as follows: frequency, 9.78 GHz; center field, 3480 G; sweep rate, 80 G/21 s; power, 20.3 mW; receiver gain, 5.02×10^4; modulation frequency, 100 kHz; time constant, 81.92 ms; modulation amplitude, 1.0 G, sweep time, 20.972 s, number of scans per spectrum, 15, and resolution, 1,024 points. EPR spectra were quantitated by peak-to-peak height of the second (low field) DMPO-OH line. Standard curves for DMPO-OH quantitation were produced by double integration of spectra with high signal-to-noise ratios [produced by using DMPO incubated with xanthine and xanthine oxidase (X/XO), data not shown]. Spectral peak areas from the X/XO standards were compared with areas of double-integrated spectra obtained (using identical EPR parameters) from standard solutions of 3-carboxy proxyl, as described previously (60). Using this method, a standard curve of peak height *vs.* nanomolar DMPO-OH was generated. Although these short scan times for experimental samples gave rise to lower signal-to-noise ratios than previously observed for isolated redoxosomes produced by longer scan times that average a greater number of spectra (28), the shorter scan times were necessary to minimize potential loss of the DMPO-OH adduct due to unknown enzymatic activity present in the samples. Additionally, since these EPR samples were run at room temperature, minimizing the scan time allowed a more accurately timed measurement after the 10-min 37°C incubation period.

Results

Cellular ROS influence TNF-α induction of IKK and NF-κB activation

Previous studies have implicated cellular ROS as important for TNF-α–mediated induction of NF-κB. Using a human mammary epithelial cell line (MCF-7 cells) that expresses undetectable levels of GPx-1 enzymatic activity (a cytosolic protein that degrades H_2O_2) (33), we first evaluated whether ectopic expression of GPx-1 could modulate transcriptional activation of NF-κB activation after TNF-α stimulation. Ectopic expression of GPx-1 from a recombinant adenoviral vector suppressed (~50%) transcriptional activation of NF-κB after TNF-α stimulation (Fig. 1A). These findings suggested that cytoplasmic H_2O_2 was important for NF-κB activation by TNF-α.

Using an alternative approach, we assessed whether the addition of antioxidant enzymes to the media at the time of TNF-α induction would also inhibit NF-κB activation. In these studies, the addition of 1 mg/ml purified SOD1 and/or catalase to the media was used to determine the contribution of both $O_2^{\bullet -}$ and H_2O_2, respectively, in the extracellular and endosomal compartments. The addition of both SOD1 and catalase together gave maximal inhibition (~50%) of NF-κB transcriptional activation by TNF-α (Fig. 1B). The addition of SOD1 alone gave no detectable inhibition, whereas catalase addition moderately inhibited NF-κB activation by TNF-α (although not to a statistically significant level). These findings suggested that both $O_2^{\bullet -}$ and H_2O_2 must be removed to effectively inhibit TNF-α activation of NF-κB. Importantly, these redox-dependent changes in NF-κB activation were mirrored by an even greater inhibition in IKK activation

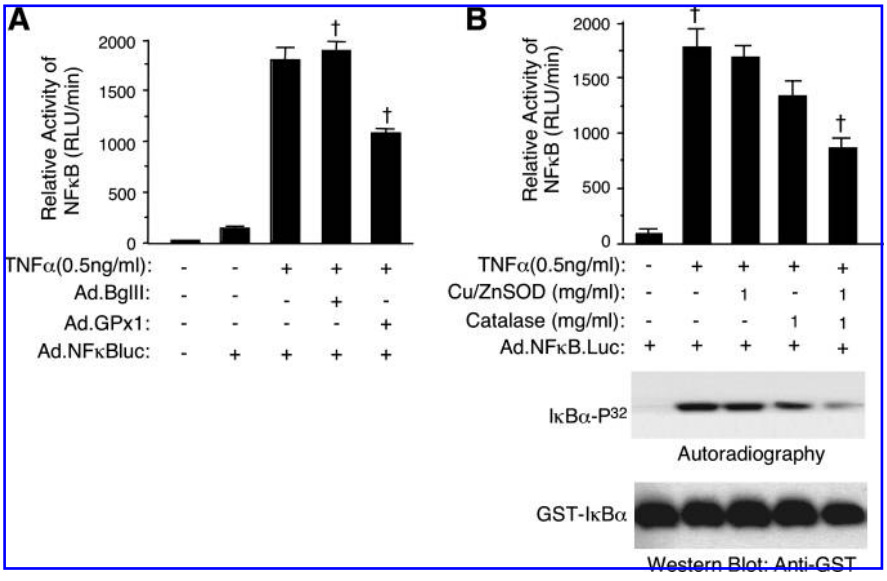

FIG. 1. TNF-α–induced NF-κB activation is redox regulated in MCF-7 cells. (**A**) MCF-7 cells were infected with the indicated adenoviral vectors (Ad.BglII is an empty viral vector control) 48 h before TNF-α treatment. NF-κB transcriptional activities were assessed at 6 h after cytokine treatment. (**B**) (*Top panel*) MCF-7 cells were treated with the indicated concentrations of purified bovine SOD1 (Cu/ZnSOD) or catalase proteins or both before TNF-α treatment, and the NF-κB transcriptional activities were evaluated at 6 h after cytokine treatment. (*Bottom panel*) IKK activity for each condition was assessed at 30 min after TNF-α stimulation by using immunoprecipitated IKK and an *in vitro* kinase assay with [γ-^{32}P]ATP and GST-IκBα. Samples were separated with SDS-PAGE, transferred to the nitrocellulose membrane, evaluated by autoradiography, and then Western blotted with anti-GST antibody. Data represent the mean ± SEM with an $n = 3$; marked comparisons (†) demonstrate significant differences with Student's *t* test ($p < 0.05$).

(Fig. 1B, lower panel); kinase activity of IKK was significantly blocked by the addition of both SOD1 and catalase to the media at the time of stimulation with TNF-α. Cumulatively, findings in Fig. 1A and B suggest that NF-κB activation after TNF-α stimulation likely has both redox-dependent and redox-independent pathways of activation and that the IKK→NF-κB component of these pathways appears to be most redox sensitive. These findings are similar to those observed in MCF-7 cells after IL-1β stimulation (32). Because this previous study implicated NADPH-dependent ROS production by the endosomal compartment as important for IL-1β–mediated activation of IKK and NF-κB, we next investigated whether endosomal ROS production might also direct TNF-α → NF-κB signaling.

TNF-α stimulates NADPH-dependent endosomal $O_2^{\bullet-}$ production required for TRAF2 recruitment to the endosomal compartment

Using Iodixanol density gradient subcellular fractionation, we investigated whether TNF-α induced NADPH-dependent generation of $O_2^{\bullet-}$ in the endosomal compartment of MCF-7 cells. This approach was previously used with MCF-7 cells to separate endosomes from other intracellular organelles also known to produce ROS (*i.e.*, mitochondria and peroxisomes) (32). Using lucigenin-based chemiluminescence assays, enriched vesicular fractions were assessed for their ability to generate NADPH-dependent $O_2^{\bullet-}$ under control (untreated) or TNF-α–stimulated conditions. As shown in Fig. 2A, TNF-α stimulation led to a substantial increase in NADPH-dependent production of $O_2^{\bullet-}$ in the endosomal fractions (Fr #2-4). The specificity of this production of $O_2^{\bullet-}$ was confirmed by using a membrane-permeable SOD mimic, MnTBAP. In the presence of MnTBAP, a significant reduction in NADPH-dependent lucigenin chemiluminescence was observed with TNF-α–stimulated endosomes (Fig. 2B). Furthermore, enhanced ROS production in the endosomal compartment after TNF-α stimulation was confirmed by endosomal loading with a membrane-impermeable BSA-conjugated $O_2^{\bullet-}$-sensitive fluorescent dye, H_2HFF-BSA (Fig. 2C). H_2HFF-BSA was previously shown to detect SOD-sensitive ROS (presumably $O_2^{\bullet-}$) in the endosomal compartment after IL-1β stimulation (32). Cumulatively, these results provide strong evidence that TNF-α activates the formation of Nox-active $O_2^{\bullet-}$-producing endosomes.

Having demonstrated that TNF-α–mediated activation of NF-κB likely involves redox activation of the endosomal compartment, we next sought to determine what aspect of TNFR1 activation might be influenced by endosomal ROS. After binding of TNF-α to TNFR1, signaling is initiated by the ordered recruitments of a number of effectors and adaptors, including TRADD, TRAF2, and RIP (36, 53). TRADD is the first effector to bind to the TNF/TNFR1 complex, followed by TRAF2 and then RIP. This series of events ultimately leads to the recruitment of IKK kinases, activation of the IKK complex, and subsequently, NF-κB activation (30). We hypothesized that endosomal ROS may facilitate docking of TNFR1 effectors on the endosome that are required for IKK activation, in a similar manner to that observed for activation of the IL-1 receptor (32). By using endosomal loading with SOD1 and catalase, we evaluated the redox dependence of the recruitment of TNFR1, TRADD, and TRAF2 to the endosomal compartment after TNF-α stimulation. Peak vesicular fractions isolated from Iodixanol gradients demonstrated substantially less TRAF2 recruitment to the endosomal compartment after TNF-α stimulation in the presence of SOD1/Catalase (Fig. 2D). This reduction closely mirrored that observed in total cellular IKK activity after SOD1/catalase loading (Fig. 1B). In contrast, endosomal loading of ROS-clearance enzymes did not alter the recruitments of TNFR1 or TRADD to the endosomal compartment after TNF-α stimulation (Fig. 2D). Additionally, biochemical studies evaluating pronase and Triton-X-100 sensitivity of ROS-clearance enzymes in isolated vesicles confirmed that the enzymes were indeed loaded into the interior of the endosomes (*i.e.*, insensitive to pronase in the absence of Triton-X-100). These findings suggested that the redox-dependent recruitment of TRAF2 to TNFR1 could be a critical step in endosomal TNF-α signaling.

Dynamin-dependent endocytosis is important for TNF-α induction of endosomal ROS and NF-κB activation

The ability of endosomally loaded SOD1 and catalase to inhibit TRAF2 recruitment to TNF-α–activated endosomes, as well as NF-κB activation (Figs. 1B and 2D), suggested that the formation of a redox-activated endosomal compartment may be critical for redox-dependent activation of the TNF receptor. Therefore, we next sought to investigate whether endocytosis was formally required for TNF-α–mediated redox-activation of NF-κB. To test this hypothesis, we used a dominant-negative dynamin mutant (K44A) to inhibit endocytosis. Overexpression of this dominant-negative dynamin (K44A) mutant has been shown to inhibit ∼75% of transferrin-mediated uptake in MCF-7 cells (32). Furthermore, the TNF receptor also appears to depend on dynamin for uptake after ligand binding (14). Expression of the dynamin mutant inhibited TNF-α induction of NF-κB by ∼40% (Fig. 3A). Furthermore, expression of dominant-negative dynamin also reduced NADPH-dependent $O_2^{\bullet-}$ production in isolated vesicular fractions by ∼66% (Fig. 3B). Because dynamin (K44A) is ∼75% effective in inhibiting endocytosis (32), these findings suggest that the majority of endosomal ROS induction after TNF-α stimulation of MCF-7 cells is likely dependent on dynamin-mediated endocytosis. In contrast, only a fraction of NF-κB activation appears to be dependent on dynamin endocytosis. We hypothesize that the dynamin-dependent fraction of NF-κB activation is redox mediated at the level of the endosome through TRAF2 recruitment and subsequent IKK activation. Such a hypothesis is consistent with the ability of SOD1 and catalase endosomal loading to more significantly inhibit IKK activation and TRAF2 recruitment, as compared with transcriptional activation of NF-κB.

TNF-α induces Nox2-dependent endosomal $O_2^{\bullet-}$

Critical to understanding endosomal mechanisms for the redox activation of the TNF receptor is the identification of the source of $O_2^{\bullet-}$-production. Because isolated endosomes could be induced to generate $O_2^{\bullet-}$ by the addition of NADPH, Nox proteins were obvious candidates. To approach this question, we first tested the sensitivity of TNF-α–induced endosomal $O_2^{\bullet-}$ production to diphenyleneiodonium (DPI; an NADPH oxidase inhibitor) and rotenone (a mitochondrial

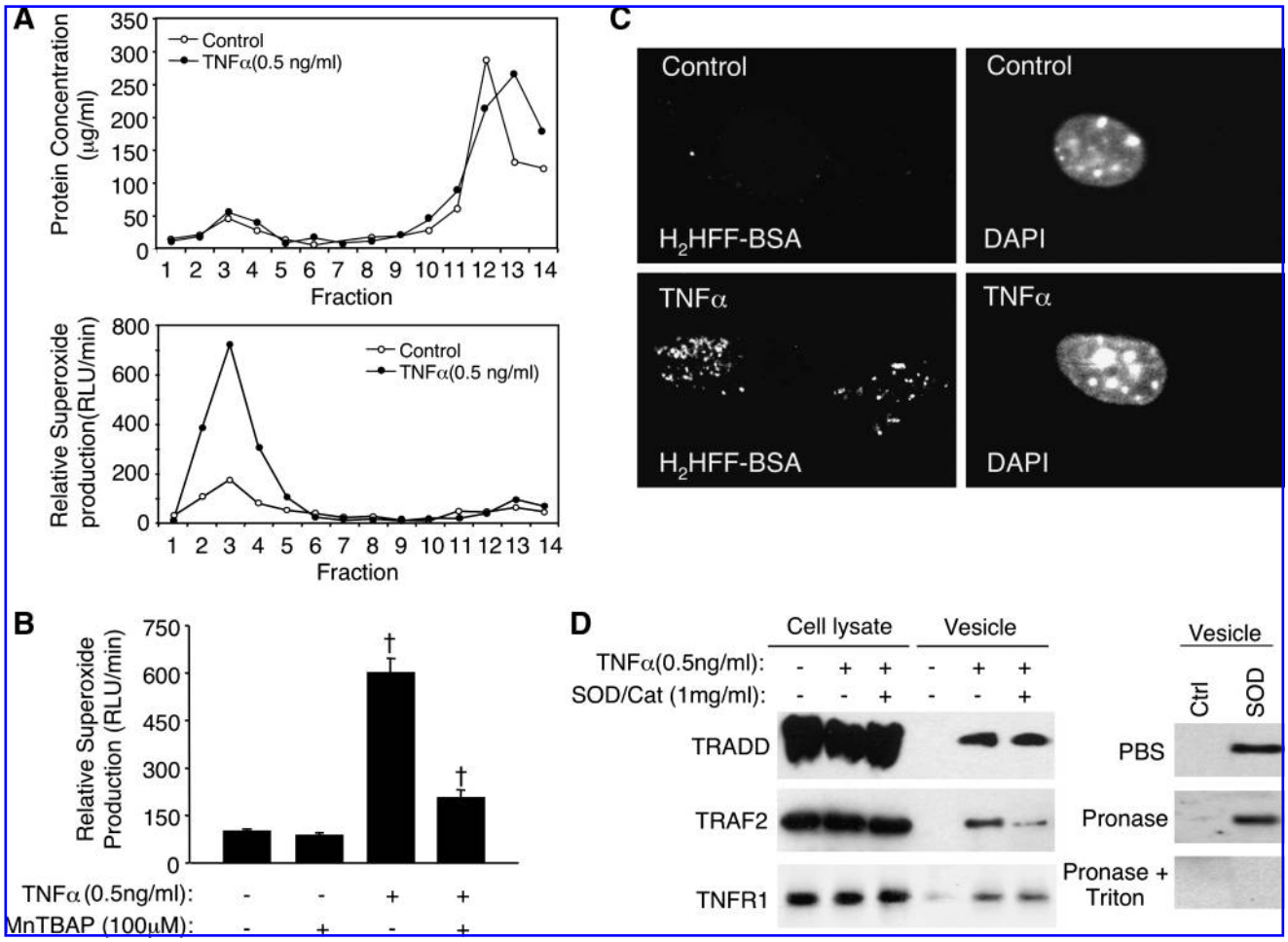

FIG. 2. TNF-α stimulates endosomal $O_2^{\bullet-}$ production required for TRAF2 recruitment. (**A**) MCF-7 cells were treated with TNF-α for 20 min, followed by vesicular fractionation using Iodixanol gradients. Each collected fraction was assayed for protein concentration (*Top panel*) or NADPH-dependent $O_2^{\bullet-}$ production using lucigenin-based chemiluminescence (*Bottom panel*). (**B**) MCF-7 cells were treated with TNF-α for 20 min, followed by vesicular fractionation on Iodixanol gradients. The pooled vesicular fractions from each sample were assayed for NADPH-dependent $O_2^{\bullet-}$ production using lucigenin-based chemiluminescence in the presence or absence of 100 μM MnTBAP. Data represent the mean ± SEM with an $n = 3$ experiments. (**C**) Endosomal $O_2^{\bullet-}$ production in primary mouse embryonic fibroblasts was visualized with H_2HFF-BSA endosomal loading in the presence of TNF-α (0.5 ng/ml) for 15 min. Control cells were treated with PBS under identical conditions. DAPI was included in the mounting media for localization of the nucleus (*right panel* in each set). H_2HFF fluorescence denotes $O_2^{\bullet-}$-production (*left panel* in each set). (**D**) (*left panel*) MCF-7 cells were loaded with purified SOD/catalase proteins and treated with TNF-α for 20 min. Whole-cell lysates and purified vesicular fractions were evaluated with Western blotting for the indicated receptor and effectors, including TNFR1, TRADD, and TRAF2. (*Right panel*) Vesicular fractions isolated from control (untreated) or SOD/Cat loaded MCF-7 cells in the absence of TNF-α. Vesicular fractions were incubated with PBS, pronase, or pronase plus Triton X-100 (0.5%) at 37°C for 30 min before analysis with Western blotting by using an anti-SOD1 antibody. Data are representative of at least three independent experiments.

electron-transport chain complex I inhibitor). These studies demonstrated that $O_2^{\bullet-}$ production in the TNF-α–induced peak vesicular fraction was sensitive only to DPI, but not to rotenone (Fig. 4A). Our previous studies evaluating redox regulation of IL-1β signaling in MCF-7 cells revealed that Nox2 was primarily responsible for endosomal production of $O_2^{\bullet-}$ and redox-dependent activation of the IL-1 receptor (32). Therefore, we hypothesized that Nox2 might also be the source of endosomal production of $O_2^{\bullet-}$ after TNF-α stimulation. To test this hypothesis, we used Nox2 siRNA, which was previously shown to significantly reduce Nox2 protein expression in MCF-7 cells (32). As shown in Fig. 4B, Nox2 siRNA, but not scrambled siRNA, attenuated TNF-α–induced endosomal NADPH-dependent production of $O_2^{\bullet-}$ in the peak vesicular fractions. Because inhibition was only partially effective with Nox2 siRNA (~40%), we also tested this hypothesis in primary dermal fibroblasts from Nox2-deficient mice (KO) and their wild-type (WT) littermates. Stimulation of WT fibroblasts with TNF-α demonstrated a similar profile of NADPH-dependent production of $O_2^{\bullet-}$ in subcellular fractions, as seen in MCF-7 cells, with the majority of $O_2^{\bullet-}$ seen in peak vesicular fractions (#2-4) enriched in endosomes (Fig. 4C and D). In contrast to WT fibroblasts, Nox2 KO fibroblasts demonstrated a lack of induction in production of $O_2^{\bullet-}$ in the peak vesicular fraction after TNF-α stimulation (Fig. 4C and D). Furthermore, in Nox2-KO fibroblasts, TNF-α–stimulated

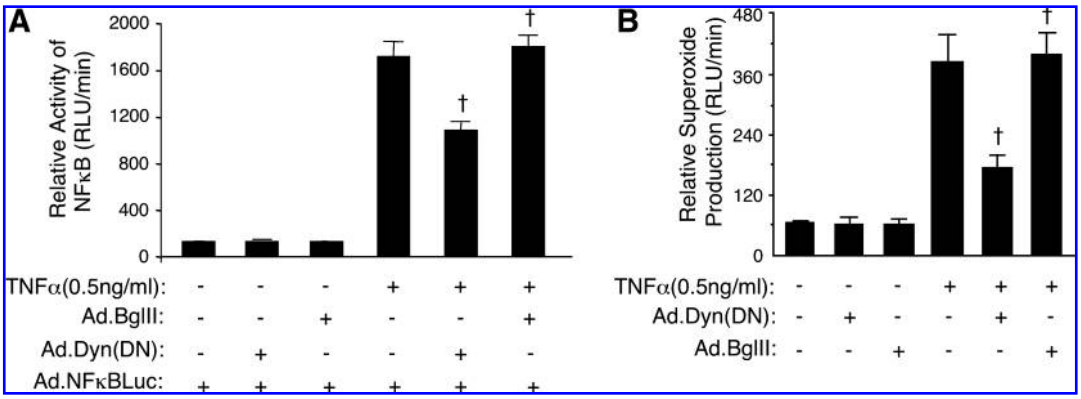

FIG. 3. Dynamin-dependent endocytosis is required for TNF-α induction of endosomal $O_2^{\bullet-}$ and NF-κB. (**A**) MCF-7 cells were infected with recombinant viral vectors before TNF-α treatment. NF-κB transcriptional activity was then assessed at 6 h after cytokine treatment. (**B**) MCF-7 cells were infected with AdDyn(DN) or Ad.BglII 48 h before cytokine treatment. Cells were then treated with TNF-α for 20 min, and vesicles were isolated on Iodixanol gradients. The pooled vesicular fraction (#2-4) was then assessed for NADPH-dependent production of $O_2^{\bullet-}$ by lucigenin-based chemiluminescence. Data represent the mean ± SEM with an $n = 3$ experiments; marked comparisons (†) demonstrate significant differences with Student's t test ($p < 0.05$).

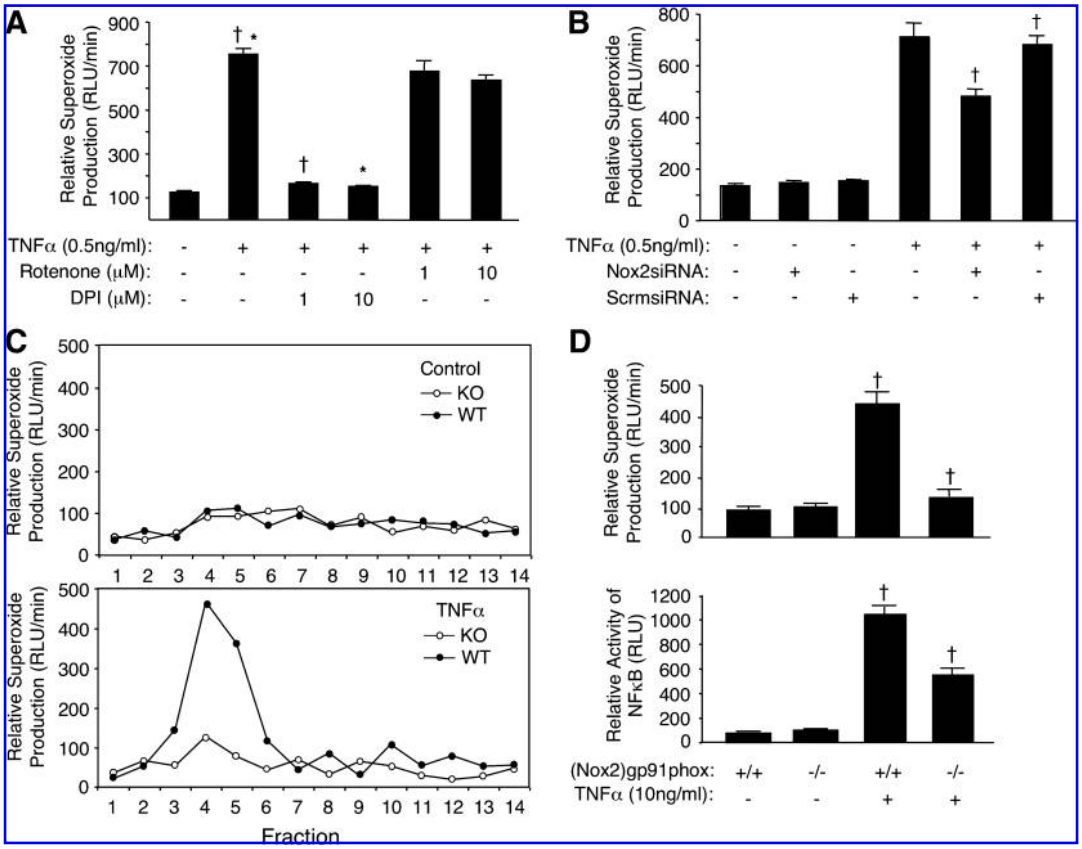

FIG. 4. Nox2 facilitates production of $O_2^{\bullet-}$ in the endosomal compartment after TNF-α stimulation. (**A**) MCF-7 cells were treated with TNF-α for 20 min, and pooled vesicular fractions (#2-4) were evaluated for NADPH-dependent production of $O_2^{\bullet-}$ in the absence or presence of DPI (NADPH oxidase inhibitor) or rotenone (mitochondrial complex I inhibitor). (**B**) MCF-7 cells were transfected with Nox2 siRNA or a scrambled (Scrm) control siRNA 48 h before TNF-α treatment for 20 min. Vesicular fractions were assayed for NADPH-dependent production of $O_2^{\bullet-}$ by lucigenin-based chemiluminescence. (**C**, **D**) Wild-type or Nox2-deficient primary mouse dermal fibroblasts were treated with or without TNF-α for 20 min, and NADPH-dependent production of $O_2^{\bullet-}$ by (**C**) individual Iodixanol gradient fractions or (**D,** *top panel*) pooled peak vesicular fractions (#3-6) was measured using lucigenin. (**D,** *bottom panel*) Wild-type or Nox2-deficient primary mouse dermal fibroblasts treated with or without TNF-α for 6 h were assayed for NF-κB transcriptional activity. Fibroblasts were infected with an NF-κB–dependent luciferase reporter recombinant adenovirus 48 h before TNF-α stimulation. Luciferase activity (as relative light units; RLUs) was then measured as an index of NF-κB transcriptional activity. Data represent the mean ± SEM with an $n = 3$ experiments; marked comparisons (*, †) demonstrate significant differences by Student's t test ($p < 0.05$).

NF-κB activation also was significantly reduced (Fig. 4D). Cumulatively, these findings strongly suggest that Nox2 is responsible for the induction of endosomal $O_2^{\bullet-}$ after TNF-α stimulation and that this ROS production influences NF-κB activation by this ligand.

TRAF2 is recruited to endosomal TNFR1 in an H_2O_2-dependent fashion

Our current findings suggest that the recruitment of TRADD to TNF-α–activated endosomes is not dependent on the endosomal redox state (Fig. 2D). In contrast, these studies also demonstrated that TRAF2 recruitment to TNF-α–activated endosomes is dependent on endosomal ROS (Fig. 2D). We therefore hypothesized that Nox2-derived ROS were necessary for the recruitment of TRAF2 to the endosomal compartment after TNF-α stimulation. Because loading of both SOD1 and catalase into endosomes was required for maximal inhibition of IKK after TNF-α stimulation, we also predicted that the ROS derived from Nox2 that facilitated TRAF2 recruitment to endosomes was likely H_2O_2 (produced by dismutation of $O_2^{\bullet-}$). To investigate these hypotheses, we sought to dissect the series of events whereby TRADD and TRAF2 are recruited to TNFR1, either in the plasma membrane or the endosomal compartments after TNF-α stimulation, and the extent to which these processes were dependent on H_2O_2.

To evaluate the recruitment of TRADD and TRAF2 to TNFR1 in the plasma membrane, we performed experiments under conditions in which cellular endocytosis was blocked (at 4°C) or significantly inhibited by adenoviral-mediated overexpression of dominant-negative dynamin. Results from these experiments (Fig. 5A) demonstrated that inhibition of endocytosis significantly impaired recruitment of TRAF2, but not TRADD, to immunoprecipitated ligand-activated TNFR1. In the absence of endocytosis at 4°C, TRAF2 recruitment to TNFR1 after TNF-α stimulation was significantly lower than that seen at 37°C. In contrast, TRADD binding to TNFR1 at 4°C was similar to that seen at 37°C in the presence of TNF-α. These findings suggested that TRADD likely recruits to TNFR1 before endocytosis, whereas recruitment of TRAF2 to TNFR1 occurs after endocytosis. This hypothesis was supported by the finding that dominant-negative dynamin expression inhibited TRAF2, but not TRADD, recruitment to TNFR1 after TNF-α stimulation (Fig. 5A).

To determine whether H_2O_2 facilitated the redox-dependent recruitment of TRAF2 to TNFR1, we tested whether TNF-α–dependent recruitment of TRAF2→TNFR1 could be reconstituted at the plasma membrane in the absence of endocytosis (*i.e.*, at 4°C) by the addition of exogenous H_2O_2. The addition of 500 μ*M* H_2O_2 effectively enhanced recruitment of TRAF2 to only ligand-activated TNFR1 at the plasma membrane at 4°C (Fig. 5B). However, the level of TRAF2→TNFR1 recruitment was still significantly less than that seen at 37°C (Fig. 5B), suggesting that other enzymatic processes reduced at 4°C also may be important for the recruitment event. These findings provided a physiologic framework for TNF-α–mediated Nox2 activation in the endosomal compartment and suggest that Nox2 may be the source of H_2O_2 required for TRAF2 recruitment to endosomal TNFR1.

Ligand-activated TNF and IL-1 receptors are selectively partitioned to Rac1-containing redox-active endosomes

Our findings that Nox2 controls H_2O_2-dependent TRAF2 recruitment to endosomal TNFR1/TRADD complexes are remarkably similar to those recently described for redox activation of the IL-1β receptor (32). In the context of IL-1β, Nox2 controls H_2O_2-dependent TRAF6 recruitment to endosomal IL-1R1/MyD88 complexes. Hence, endocytosis of IL-1R1 and TNFR1 into a redox-active endosomal compartment appears to spatially control the H_2O_2-dependent recruitment of TRAFs to their cognate ligand-activated receptor complexes. We hypothesized that these redox-active signaling endosomes would share similar redox-modulator proteins, while also retaining specific factors required for the activation of their receptors (*i.e.*, TNFR1 and IL-1R1). To formally demonstrate such a hypothesis holds, we sought to directly evaluate whether specific ligand signals (TNF-α and IL-1β) direct their cognate receptor to biologically similar Nox-active endosomes, while retaining specificity for redox-dependent recruitment of receptor-specific TRAFs.

To directly evaluate whether redox-active endosomes harbor intracellular pools of activated ligand/receptor complexes, we attempted selectively to purify Nox2-active endosomes using immuno-affinity isolation and HA-tagged Rac1. Because Rac1 is an essential Nox2 activator, we reasoned that Rac1-bound endosomes would be enriched for Nox activity and other components potentially specific to redox-active endosomes and the ligand-activated receptor. HA-Rac1–containing endosomes were isolated from untreated, TNF-α–, or IL-1β–induced MCF-7 cells. After immunoisolation, the HA-Rac1–bound and –unbound vesicular fractions were then assessed for enrichment of HA-Rac1, $p67^{phox}$, SOD1, TNFR1, TRAF2, IL-1R1, and TRAF6, in relation to the common early endosomal marker, Rab5. Both $p67^{phox}$ (an essential activator

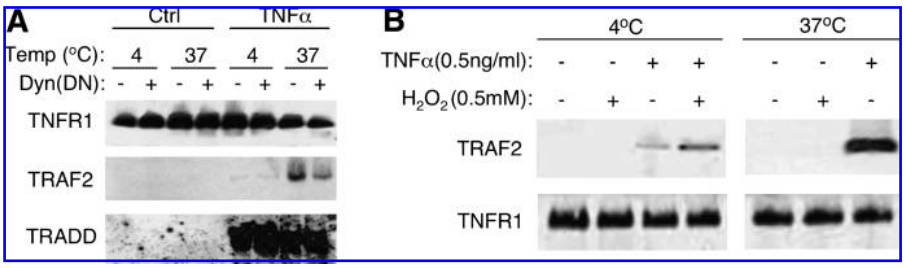

FIG. 5. TRAF2 recruitment to endosomal TNFR1 is dependent on H_2O_2. (**A**) MCF-7 cells were infected with Ad.Dyn(DN) or Ad.BglII (negative control). At 48 h after infection, cells were treated with TNF-α at either 4°C (for 1 h) or 37°C (for 20 min). TNFR1 was then immunoprecipitated, followed by Western blotting for the indicated proteins. (**B**) MCF-7 cells were treated with TNF-α at 4°C (for 1 h) or 37°C (for 20 min) in the presence or absence of H_2O_2. TNFR1 was then immunoprecipitated, followed by Western blotting for the indicated proteins. Data are representative of at least three independent experiments.

of Nox2) and SOD1 were recently found to recruit to IL-1β–stimulated redox-active endosomes (32, 42).

Findings from these studies demonstrated that HA-Rac1 incorporation into crude vesicular fractions was significantly enhanced by both IL-1β (lane 4) and TNF-α (lane 7) stimulation (Fig. 6A). Rac1 was found only at low levels in unstimulated vesicles (lane 1). These findings support the notion that Rac1 (an essential activator of Nox2) is specifically recruited to the endosomal compartment after both IL-1β and TNF-α stimulation. Immunoaffinity isolation of HA-Rac1–bound endosomes demonstrated that the purification procedure was capable of isolating ~75% of the HA-immunoreactive endosomes (lane 5 *vs*. 6 and 8 *vs*. 9). As anticipated, this fractional enrichment for HA-Rac1 in the anti-HA-bound pellet mirrored the enrichment seen in its capacity to produce $O_2^{\bullet -}$. Similarly, the enrichment of SOD1 and $p67^{phox}$, relative to a general endosomal marker (Rab5), was also seen. In the absence of TNF-α or IL-1β stimulation, SOD1 and $p67^{phox}$ failed to recruit to endosomal membranes (lane 1). Most important, recruitment of IL-1R1/TRAF6 or TNFR1/TRAF2 to Rac1-containing endosomes was specific to IL-1β or TNF-α stimulation, respectively (Fig. 6, lane 5 *vs*. 8). No IL-1R1/TRAF6 was recruited to Rac1-containing endosomes after TNF-α stimulation (lane 8). Similarly, no TNFR1/TRAF2 was recruited to IL-1β–activated, Rac1-containing endosomes (lane 5). These findings provide direct evidence for the enrichment of ligand-activated receptors and their TRAF effectors in redox-active endosomes.

Estimating the capacity of redox-active signaling endosomes to produce $O_2^{\bullet -}$

Quantifying levels of $O_2^{\bullet -}$ is challenging, given the unstable nature of this reactive oxygen species. Nonetheless, when thinking about the mechanisms by which redox-active endosomes transmit their ROS signals, having an estimate of the flux of $O_2^{\bullet -}$ production at the level of the endosome would be very useful. To this end, we attempted to estimate the flux of $O_2^{\bullet -}$ generated by TNF-α–stimulated redox-active endosomes. To simplify the discussion on this topic, we use the terminology set forth in a Forum Review of this issue of *ARS* (46), which classifies signaling *redox*-active end*osomes* as *redoxosomes*. We present data here that utilize EPR with DMPO standard curves to estimate the flux of $O_2^{\bullet -}$ produced by

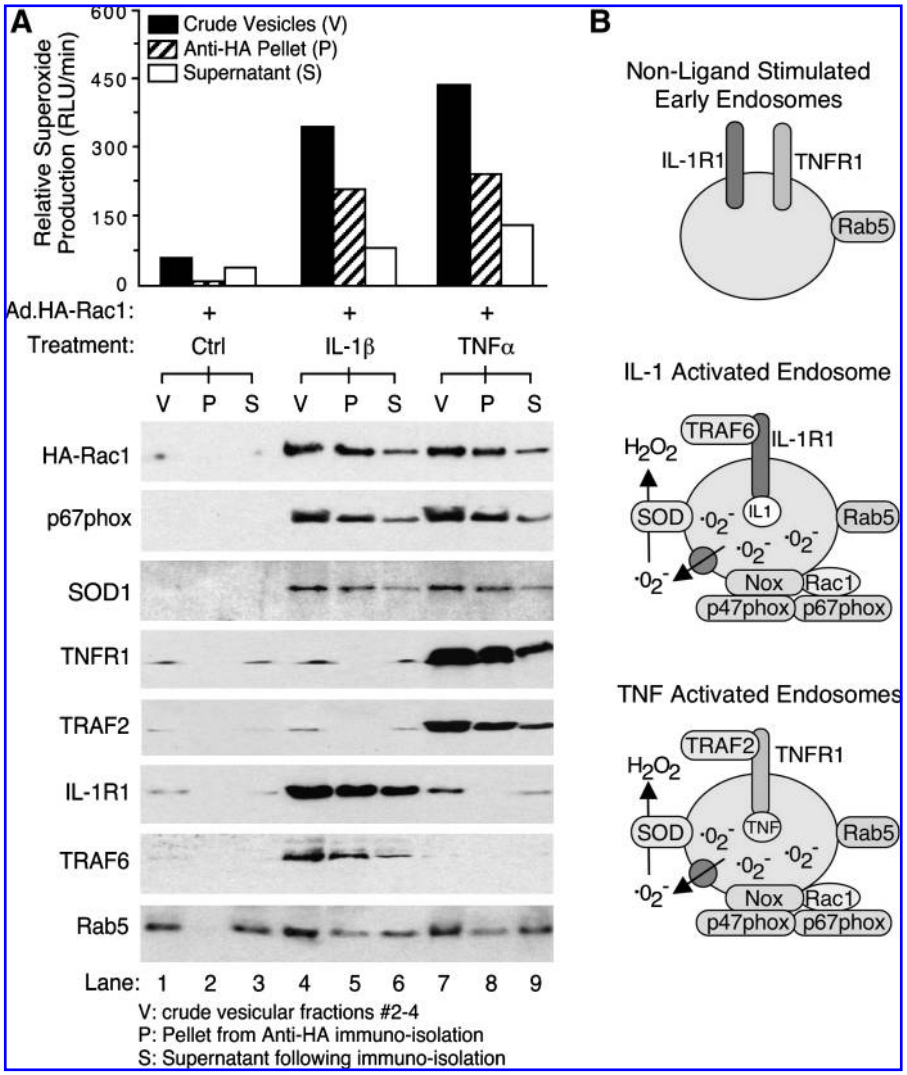

FIG. 6. TNF-α and IL-1β induce redox-active Rac1-containing endosomes that partition TRAF recruitment to their cognate receptors. (**A**) Ad.HA-Rac1–infected MCF-7 cells were stimulated with TNF-α (0.5 ng/ml) or IL-1β (1 ng/ml) for 20 min, and vesicular fractions were isolated. Half of the crude combined vesicular peak fractions (#2–4) were used for immunoaffinity isolation of HA-Rac1–associated endosomes by using anti-HA–bound Dynabeads. The crude vesicular sample (V), immunoisolated pellets (P), and supernatants (S) were evaluated for NADPH-dependent production of $O_2^{\bullet -}$ and Western blotting for the indicated proteins. Values for production of $O_2^{\bullet -}$ give the total activity in each sample (V, P, or S). An equal percentage of each sample (V, P, or S) was loaded in each Western blot lane. Data are representative of at least three independent experiments. (**B**) Schematic summary of vesicular proteins recruited to IL-1β– or TNF-α–stimulated, redox-active endosomes. The presence of an $O_2^{\bullet -}$ channel and IL-1β/IL-1R1–related data is inferred from other publications on this topic (32, 42). The recruitment of adaptors/effectors other than TRAF to IL-1R1 or TNFR1 is recognized, but not shown.

isolated populations of endosomes containing redoxosomes. Both TNF-α–stimulated and –unstimulated endosomes were evaluated and the difference in NADPH-dependent $O_2^{\bullet-}$ was designated as derived from newly formed redoxosomes. These calculations require several parameters and assumptions to calculate the flux of $O_2^{\bullet-}$ including (a) number of cells in the starting material, (b) number of redoxosomes per cell, (c) loss of endosomes during the isolation period, and (d) the diameter and volume of redoxosomes. The values used for each of these parameters and assumptions are given in Table 1.

EPR was used to estimate $O_2^{\bullet-}$ production by isolated TNF-α–stimulated redoxosomes. MCF-7 cells, treated with or without TNF-α (0.5 ng/ml), were harvested at 20 min after stimulation and endosomes were isolated on Iodixanol gradients. To estimate the loss of endosomes during the isolation procedure, MCF-7 cells were loaded with biotin-transferrin, and an equal percentage of the starting material for both PNS and Iodixanol endosomal fractions was evaluated by Western blot for biotin-transferrin content and quantified (Fig. 7A). Using this approach, it was calculated that 63% of the endosomal fraction was lost during the preparation procedure (Fig. 7A). Hence, a yield of 37% was used to correct for the final values of $O_2^{\bullet-}$ flux. Endosomes isolated from 1.0×10^6 MCF-7 cells were incubated with DMPO (in the presence and absence of 100 μM NADPH) at 37°C for 10 min and then examined by EPR (Fig. 7B). The peak height of the EPR signal was then correlated with standard curves of DMPO-OH to calculate the concentration of $O_2^{\bullet-}$ in each sample (Fig. 7C). As shown in Fig. 7C, control unstimulated endosomes gave a background level of production of $O_2^{\bullet-}$ in the presence of NADPH. This level was not significantly different from that of TNF-α–stimulated endosomes not treated with NADPH. However, $O_2^{\bullet-}$-production by TNF-α–induced endosomes treated with NADPH increased threefold in comparison to the two background controls (Fig. 7C). The difference in values for NADPH-treated control *vs*. NADPH-treated TNF-α–induced endosomes was used to calculate the moles of $O_2^{\bullet-}$ generated by redoxosomes derived from 1.0×10^6 cells. This value was then corrected for the loss of endosomes in the isolation (63%). Based on the estimated number of redoxosomes per cell and the volume of a redoxosome (Table 1), estimates of the NADPH-dependent capacity to produce $O_2^{\bullet-}$ per redoxosome and per cell could be made (Table 2). These calculations took into account the 10-min reaction period and the assumption that the rate of production of $O_2^{\bullet-}$ was constant over that time. With these calculations, the rate of TNF-α–stimulated redoxosomal production of $O_2^{\bullet-}$ was estimated to be 4.3×10^{-22} moles redoxosome^{-1}s^{-1}, which is equal to ~260 molecules of $O_2^{\bullet-}$ redoxosome^{-1}s^{-1}. The errors in these calculations were $\pm1.2\times10^{-22}$ moles redoxosome^{-1}s^{-1} and ±74 $O_2^{\bullet-}$ molecules redoxosome^{-1}s^{-1}. By using an estimated diameter of 200 nm for an early endosome/redoxosome, which has a volume of 4.2×10^{-18} L, one can then calculate the flux in terms of molar concentration of $O_2^{\bullet-}$ produced per second for a redoxosome (Ms^{-1}). The value for the flux of $O_2^{\bullet-}$ in a single 200-nm-diameter TNF-α–stimulated redoxosome was estimated to be 1.0×10^{-4} Ms^{-1} at pH 7.4, with an error of $\pm0.3\times10^{-4}$ Ms^{-1}.

For these calculations of flux, it is important also to consider the efficiency by which DMPO-OH detects $O_2^{\bullet-}$. It was previously reported that this efficiency may be as low at 27% in a "clean" system (55). It is very difficult to estimate the efficiency with which DMPO-OH reports the production of superoxide in a complex biologic system since the efficiency of DMPO-OOH conversion to DMPO-OH is greatly enhanced by biologic molecules such as peroxidases. Unlike DMPO-OOH, DMPO-OH is relatively stable, so the rate of conversion of DMPO-OOH to DMPO-OH would influence the estimates of redoxosomal flux of $O_2^{\bullet-}$ in our studies, and biologic molecules in the sample might make this process relatively efficient. However, given previous studies on the efficiency of DMPO to detect $O_2^{\bullet-}$ in a clean system (55), redoxosomal $O_2^{\bullet-}$ flux may actually be three- to fourfold higher than estimated in our experiments. Another variable to consider is changes in redoxosome size; our estimates for the flux of $O_2^{\bullet-}$ are based on a diameter of 200 nm (Table 1). This estimate is consistent with the literature for early endosomes (7, 8, 28, 43) and with our own studies evaluating redoxosomes by EM (42). However, endosome size is very dynamic and changes rapidly as endosomes traffic and fuse with other compartments. Since endosomal volume changes with the cube of the radius, the actual flux of $O_2^{\bullet-}$ will change rapidly as the size of an endosome changes. For example, a 750-nm redoxosome, which is closer to the size of a late endosome (16), would have a flux of $O_2^{\bullet-}$ 53-fold lower (1.9×10^{-6} Ms^{-1}) than a 200-nm redoxosome (1.0×10^{-4} Ms^{-1}) at pH 7.4. Hence, depending on the actual size of functioning redoxosomes, which is still a very open question, the NADPH-dependent $O_2^{\bullet-}$ flux may fall between these two values at neutral pH.

When translating these estimates of superoxide-producing capacity of redoxosomes to a biologic perspective, it is important to note that they do not take into account the rate of spontaneous dismutation of $O_2^{\bullet-}$. Furthermore, in the EPR assay used above, it is assumed that the concentration of

Table 1. Parameters and Assumptions for Calculating Redoxosomal Flux of $O_2^{\bullet-}$

Parameter/Assumption	*Starting number of cells*	*No. of redoxosomes per cell*[a]	*Efficiency of endosomal isolation (loss)*[b]	*Diameter (volume) of a redoxosome*[c]
Value	1.0×10^6 cells	100	37% (63%)	200 nm(4.2×10^{-18} L)
Data or reference for value	NA	Fig. 2C	Fig. 7	(7, 8, 28, 42, 43)

[a]The number of redoxosomes per cell following TNF stimulation was estimated from H_2HFF-BSA loading, as shown in the cited figure.
[b]During the endosomal preparations, the yield (or loss of endosomes) was calculated by using a biotin-transferrin uptake assay as described in Methods and presented in the cited figure.
[c]The diameter of redoxosomes was estimated based on electron micrographs of isolated IL-1–stimulated redoxosomes containing IL-1R1 and general size parameters for the early endosomal compartment (see referenced articles). These studies suggest that early endosomes are ~100–300 nm in diameter.

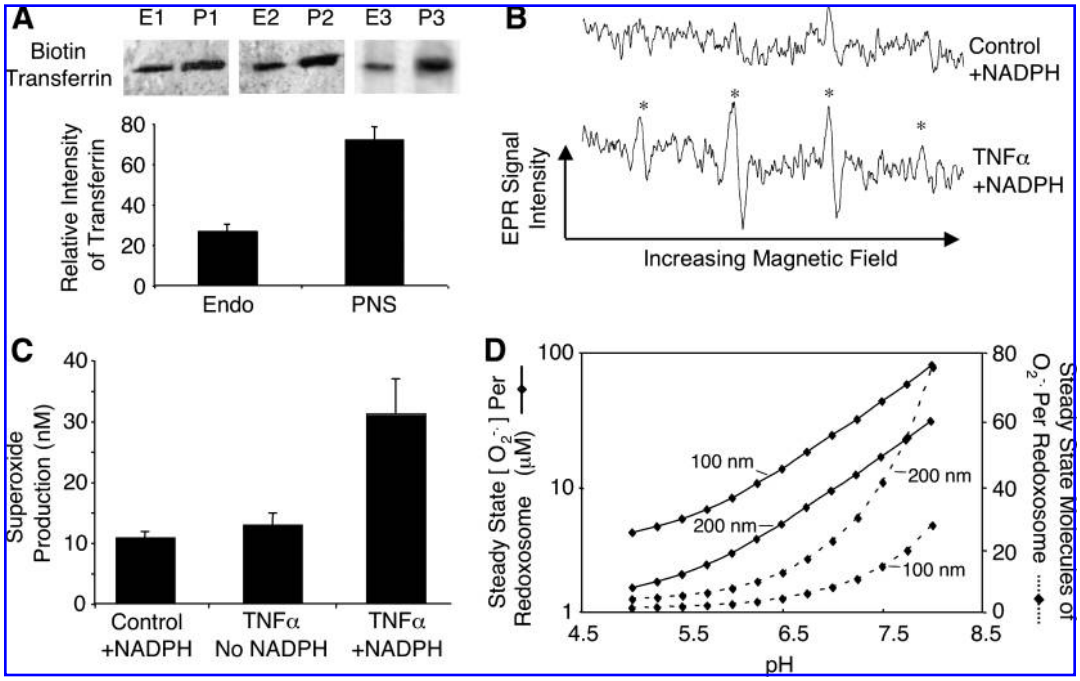

FIG. 7. Estimates of production of $O_2^{\bullet-}$ by TNF-α–activated redoxosomes. (**A**) Estimates of endosomal loss during isolation on Iodixanol gradients with biotin-transferrin uptake. MCF-7 cells were loaded with biotin-transferrin, and postnuclear supernatants (PNS) were generated. PNS was then loaded onto Iodixanol gradients, and peak endosomal fractions were isolated. (*Upper panel*) An equal percentage of the starting sample for both the PNS (P1, P2, and P3) and peak endosomal fractions (E1, E2, and E3) was loaded on an SDS-PAGE gel and Western blotted with streptavidin linked to an infrared dye. Lanes show fractions from three independent experiments. (*Lower panel*) Quantification of Western blot results in the upper panel using infrared scanning. (**B**) Averaged EPR spectra from three independent samples of unstimulated and TNF-α–stimulated endosomes in the presence of NADPH. These spectra were generated by averaging the 15 scans from each of three samples for each condition, giving rise to the 45 scan-averaged spectra, as shown. Asterisks mark the DMPO-OH radical EPR signature. (**C**) Quantification of EPR data for isolated endosomal preparations under the indicated conditions. Data represent the mean ± SEM for $n = 3$ independently isolated samples for each group. (**D**) Theoretical calculation of the steady-state molar concentration and molecules of $O_2^{\bullet-}$ in TNF-α–stimulated redoxosomes as a function of changing pH. These estimates of the superoxide-producing capacity of redoxosomes take into account the spontaneous dismutation rates of $O_2^{\bullet-}$ at various pH values for both 100- and 200-nm (diameter) redoxosomes, as marked.

50 m*M* DMPO is sufficient to outcompete the spontaneous dismutation of $O_2^{\bullet-}$. At pH 7.4, the observed second-order rate constant for spontaneous dismutation of $O_2^{\bullet-}$ is 2.5×10^5 Ms^{-1}. This rate constant significantly increases at lower pH ($k_{obs} = 6.2\times10^6\ Ms^{-1}$ at pH 6.0; $k_{obs} = 2.1\times10^7\ Ms^{-1}$ at pH 5.0) (5), resulting in a significantly shorter half-life for $O_2^{\bullet-}$ at lower pH. Based on previous studies, the pH inside certain types of endosomal compartments can significantly decrease to as low as 5.0–6.0 for the late endosome and lysosome (4). To appreciate the potential effect of changing endosomal pH on the production of $O_2^{\bullet-}$ by redoxosomes, we estimated the steady-state concentration of $O_2^{\bullet-}$ inside the redoxosome ($[O_2^{\bullet-}]_{steady\text{-}state}$) by taking into account the rates of production and spontaneous dismutation at various pH values (Fig. 7D). These calculations assume that the production of $O_2^{\bullet-}$ is not affected by pH changes, an assumption that we recognize is likely false, but at present is not possible to evaluate. Using the formulas and rate constants in Table 3, the steady-state molar concentration of $O_2^{\bullet-}$ inside the redoxosome was calculated for pH values ranging from 5.0 to 8.0. These calculations were used to estimate the theoretical change in the steady-state level of $O_2^{\bullet-}$ inside the redoxosome as a function of pH (Fig. 7D). As seen in this figure, lumenal pH of the endosomal compartment will significantly influence the abundance of $O_2^{\bullet-}$, as well as the dismutation product, hydrogen peroxide. At a pH of 7.4 for a 200-nm redoxosome, the steady-state concentration of $O_2^{\bullet-}$ is estimated to be 14 μM, and this is predicted to decrease to 1.5 μM at a pH of 5.0. When one superimposes potential changes in redoxosomal size (from 100 to 500 nm) with potential changes in lumenal pH,

Table 2. Estimates for TNF-α–Stimulated Redoxosomal Generation of $O_2^{\bullet-}$

Raw data: moles $O_2^{\bullet-}s^{-1}$ (1.0×10^6 cells)	*Moles $O_2^{\bullet-}$ $cells^{-1}s^{-1}$*	*Moles $O_2^{\bullet-}$ $redoxosome^{-1}s^{-1}$*	*$O_2^{\bullet-}$ molecules $redoxosome^{-1}s^{-1}$*	*$O_2^{\bullet-}$ flux per redoxosome (Ms^{-1})*
$4.3\times10^{-14} \pm 1.2\times10^{-14}$	$4.3\times10^{-20} \pm 1.2\times10^{-20}$	$4.3\times10^{-22} \pm 1.2\times10^{-22}$	260 ± 74	$1.0\times10^{-4} \pm 0.3\times10^{-4}$

All values were determined at pH 7.4, and flux measurements assume that the diameter of a redoxosomes is ~200 nm.

Table 3. Predicted Changes in Redoxosomal Concentration of $O_2^{\bullet-}$ as a Function of Endosomal pH and Size

	Endosome diameter	*pH 8.0*	*pH 7.4*	*pH 7.0*	*pH 6.0*	*pH 5.0*
k_{obs} (Ms^{-1})	NA	5.6×10^{4}	2.5×10^{5}	6.7×10^{5}	6.2×10^{6}	2.1×10^{7}
$[O_2^{\bullet-}]_{steady\text{-}state}$ (M)	100 nm	8.6×10^{-5}	4.1×10^{-5}	2.5×10^{-5}	8.1×10^{-6}	4.4×10^{-6}
	200 nm	3.0×10^{-5}	1.4×10^{-5}	8.6×10^{-6}	2.8×10^{-6}	1.5×10^{-6}
	300 nm	1.7×10^{-5}	7.8×10^{-6}	4.8×10^{-6}	1.6×10^{-6}	8.5×10^{-7}
	500 nm	7.7×10^{-6}	3.6×10^{-6}	2.2×10^{-6}	7.3×10^{-7}	4.0×10^{-7}

Equation used for calculations: $[O_2^{\bullet-}]_{steady\text{-}state} = (F_0/2k_{obs})^{0.5}$.
k_{obs}, Observed spontaneous dismutation rate constant for $O_2^{\bullet-}$ (Ms^{-1}) as a function of changing pH (5); F_0, initial rate of generation of $O_2^{\bullet-}$ (Ms^{-1}) from Table 2; $[O_2^{\bullet-}]_{steady\text{-}state}$, steady-state concentration of $O_2^{\bullet-}$ in redoxosomes (M).

the steady-state concentration of $O_2^{\bullet-}$ within redoxosomes could dynamically change more than two orders of magnitude (Table 3). For example, a 500-nm redoxosome at pH 5.0 would be estimated to have a steady-state lumenal concentration of $O_2^{\bullet-}$ of 0.40 μM, whereas for a 100-nm redoxosome at pH 7.4 the value would be 41 μM.

Discussion

These studies assessing the redox dependence of TNF-α–mediated NF-κB activation demonstrate that endocytosis of TNFR1 and the production of endosomal ROS facilitates TRAF2 recruitment to the TNFR1/TRADD receptor complex to activate IKK. This redox-dependent TNF-α pathway shares interesting similarities with those previously observed for the IL-1β pathway (32). First, both appear to be dependent on Nox2-mediated ROS production in the endosomal compartment. Second, the redox-dependent event that controls activation of both IL-1R1 and TNFR1 appears to involve recruitment of TRAFs. Third, both receptor pathways recruit SOD1 to ligand-activated redoxosomes containing Rac1 and $p67^{phox}$. In this context, redoxosomes for these two independent receptor pathways appear uniquely equipped to carry out $O_2^{\bullet-} \rightarrow H_2O_2$ production at intracellular locations where ligand-activated receptors are concentrated.

The induction of redoxosomes after TNF-α or IL-1β stimulation provides a framework for understanding how ROS can influence receptor activation. Findings from our present study have now implicated H_2O_2 as a molecular signal for the recruitment of TRAF2 to the TNFR1 complex at the surface of the endosome. This finding is consistent with another study demonstrating that TRAF2-deficient mouse embryonic fibroblasts (MEFs) are resistant to ROS-induced cell death when compared with their wild-type cells (54); reconstitution of TRAF2 expression in TRAF2-deficient MEFs also restored sensitivity to ROS-induced cell death. Although our present study and this previous work suggest that TRAF2 function is responsive to redox stress, the molecular mechanism whereby TRAF2 is regulated by ROS remains unclear. We hypothesize that H_2O_2 may modify reactive thiol groups at certain cysteines within TRAF2, allowing its docking on the TNFR1/TRADD complex. In this context, thiol-modifying agents have been shown to inhibit TRAF2-mediated activation of the SAPK/JNK pathway (44, 45). Alternatively, Nox-dependent H_2O_2 could potentially modify TRAF2 function through the inhibition of cellular phosphatases, as previously shown for other redox-dependent systems (49). Although the functional significance of TRAF2 phosphorylation has been debated, recent studies have suggested that TRAF2 phosphorylation is important for CD40 signaling, as well as TNF-α–induced NF-κB activation (9, 20, 34). Of interest, Thr117 in TRAF2 is phosphorylated after TNF-α stimulation, and dephosphorylation of TRAF2 by the phosphatase PP2A holoenzyme inhibits NF-κB activation (34). Given that the PP2A holoenzyme forms a complex with TRAF2 (34), it also seems plausible that endosomal induction of H_2O_2 could enhance TRAF2 phosphorylation and activation by inhibiting TRAF2-associated protein phosphatases, such as PP2A.

Our studies have implicated Rac1-regulated Nox2 as a source of endosomal ROS after TNF-α stimulation. However, it appears that other Rac1-regulated Nox complexes may also serve in this context. For example, in vascular smooth muscle cells, Nox1 (which is also regulated by Rac1) appears to facilitate the induction of cellular ROS important for NF-κB activation after TNF-α stimulation (41). It is presently unclear how Nox is recruited into endosomes after TNF-α stimulation; however, studies on IL-1β endosomal activation pathways implicate Rac1 in the recruitment process (32). In the context of TNF-α, a recent study demonstrated that Nox1 associates with Rac1/TRADD/RIP complexes after TNF-α stimulation to facilitate redox-dependent necrotic death in mouse fibroblasts (27). In these studies, RIP was required for the recruitment of Nox1 to TRADD complex, but Rac1 was also required for the induction of cellular ROS. Although these studies did not evaluate the direct association of Nox1 with TNFR1 or the formation of redoxosomes, the time course of ROS production in these studies is consistent with the involvement of Nox1 in an early endosomal compartment harboring TNFR1. Hence, RIP may also be a candidate for recruitment of Nox2 to redoxosomes after TNF-α stimulation.

The finding that Nox1-dependent cellular ROS after TNFα stimulation plays an important role in necrotic cell death of primary mouse embryonic fibroblasts (27) is contrasted to findings in this report demonstrating that Nox2 facilitates NF-κB activation by TNF-α in primary dermal fibroblasts. Such differences may simply be due to the cellular origin of the fibroblasts and differential expression of Nox isoforms, or they may imply a more complex redox-dependent regulation of TNFR1 that facilitates cell death or NF-κB activation. Activation of TNFR1 has been shown to form both membrane-bound and soluble complexes that differentially regulate survival through NF-κB activation and apoptosis, respectively (22, 40). Whether these two distinct complexes differentially associate with different Nox isoforms remains to be determined.

The level of ROS production stimulated in the endosomal compartment following TNF-α stimulation has important potential implications for mechanisms of redox-signaling

through TNFR1. The value for EPR-estimated redoxosomal $O_2^{\bullet-}$ flux of 100 μMs^{-1} seems very high at face value. However, when one considers the small volume of an endosome and the total $O_2^{\bullet-}$ produced per cell, this value takes on a new perspective. For example, the overall rate of $O_2^{\bullet-}$ generated theoretically by all redoxosomes in a single TNF-α–activated MCF-7 cell (4.3×10^{-20} moles $O_2^{\bullet-}$ $cell^{-1}s^{-1}$, assuming 100 redoxosomes per cell) is still ~2,000-fold lower than the rate of generation of $O_2^{\bullet-}$ by a single phagocyte. Neutrophils generate $O_2^{\bullet-}$ at a rate between 5.0×10^{-17} and 17×10^{-17} moles $O_2^{\bullet-}$ $cell^{-1}s^{-1}$ (11, 26, 52, 61), which translates to an estimated $O_2^{\bullet-}$ flux of 2.5 mMs^{-1} within a single phagosome (61). This estimated $O_2^{\bullet-}$ flux for a phagosome is ~25-fold higher than that for a 200-nm TNF-α–activated redoxosome (0.1 mMs^{-1}).

Based on the similar mechanisms that facilitate TNF-α– and IL-1β–induced NF-κB activation through endosomal activation of Nox, we hypothesize that redoxosomes may play important roles in the activation of redox-dependent receptors. The activation of several receptors in addition to IL-1Rs and TNFR1 has been demonstrated to have redox-signaling components. For example, ligands such as lipopolysaccharide (LPS) (24, 51), angiotensin II (18), platelet-derived growth factor (PDGF) (56), and insulin (37) all have redox-dependent components in their signaling consistent with Nox activation at the endosomal level. To this end, we propose that redoxosomes encompass a subset of signaling endosomes that use local Nox-derived ROS to facilitate receptor-signaling events.

Based on the findings from this study and others, several common redoxosomal components have been identified (Fig. 6B). These include Nox complex components (Nox1 or Nox2, Rac1, $p47^{phox}$, $p67^{phox}$), SOD1, and an unidentified DIDS-sensitive $O_2^{\bullet-}$ channel (32, 41, 42). Although it is currently unclear whether $O_2^{\bullet-}$ channels also exist in TNF-α–activated redoxosomes, given the similarities seen in the redox-dependent TRAF recruitment to IL-1R1 and TNFR1 in MCF-7 cells, it is likely that such a channel exists in redoxosomes activated by both TNF-α and IL-1β. The common finding of SOD1 recruitment to both TNF-α– and IL-1β–activated redoxosomes also suggests that SOD1 may play an active role in $O_2^{\bullet-}$ dismutation at the surface of the endosome. Such SOD1 functions may be important for mediating localized H_2O_2-directed signaling events and/or the redox-sensitive control of Rac1-regulated Nox complexes, as recently described (19).

Acknowledgments

This work was supported by NIDDK (RO1 DK067928 and DK051315), the vector core funded through the Center for Gene Therapy (P30 DK54759), and the Roy J. Carver Chair in Molecular Medicine. We also gratefully acknowledge the support of The University of Iowa ESR Facility and Dr. Christine Blaumueller for editorial assistance.

Abbreviations

BSA, bovine serum albumin; DAPI, 4′, 6′-diamidino-2-phenylindole; DMPO, 5,5-dimethyl-1-pyrroline *N*-oxide; DPI, diphenyleneiodonium; DTPA, diethylenetriaminepentaacetic acid; Duox, dual oxidase; EDTA, ethylenediaminetetraacetic acid; EGF, epidermal growth factor; FBS, fetal bovine serum; GPx1, glutathione peroxidase 1; GST, glutathione-s-transferase; HA, influenza A viral hemagglutinin (tag); HEPES, 4-(2-hydroxyethyl)-1-piperazineethanesulfonic acid; (H_2HFF)-BSA, dihydro-2′,4,5,6,7,7′-hexafluorofluorescein-bovine serum albumin; H_2O_2, hydrogen peroxide; IL-1β, interleukin-1β; IL-1R1, interleukin-1 receptor 1; IKK, IκB kinase; JNK, C-Jun N-terminal kinase; LPS, lipopolysaccharide; MEF, mouse embryonic fibroblast; MOI, multiplicity of infection; MyD88, myeloid differentiation primary response gene (88); NADPH, nicotinamide–adenine dinucleotide phosphate (reduced); NF-κB, nuclear factor κB; Nox, NADPH oxidase; $O_2^{\bullet-}$, superoxide; PBS, phosphate-buffered saline; PDGF, platelet-derived growth factor; PNS, postnuclear supernatant; PP2A, protein phosphatase 2A; Rac1, Ras-related C3 botulinum toxin substrate 1; RIPA, radioimmunoprecipitation assay; RIP, receptor-interacting protein; ROS, reactive oxygen species; SAPK, stress-activated protein kinase; SDS-PAGE, sodium dodecylsulfate–polyacrylamide gel electrophoresis; SOD1, superoxide dismutase 1; siRNA, small interfering RNA; TNF-α, tumor necrosis factor α; TNFR1, tumor necrosis factor receptor 1; TRAF2, tumor necrosis factor receptor-associated factor 2; TRADD, tumor necrosis factor receptor-associated death domain.

Disclosure Statement

No competing financial interests exist.

References

1. Anilkumar N, Weber R, Zhang M, Brewer A, and Shah AM. Nox4 and nox2 NADPH oxidases mediate distinct cellular redox signaling responses to agonist stimulation. *Arterioscler Thromb Vasc Biol* 28: 1347–1354, 2008.
2. Bae YS, Kang SW, Seo MS, Baines IC, Tekle E, Chock PB, and Rhee SG. Epidermal growth factor (EGF)-induced generation of hydrogen peroxide: role in EGF receptor-mediated tyrosine phosphorylation. *J Biol Chem* 272: 217–221, 1997.
3. Baeuerle PA and Baltimore D. NF-kappa B: ten years after. *Cell* 87: 13–20, 1996.
4. Barriere H and Lukacs GL. Analysis of endocytic trafficking by single-cell fluorescence ratio imaging. *Curr Protoc Cell Biol* Chapter 15: Unit 15 13, 2008.
5. Bielski BHJ, Cabelli DE, Arudi RL, and Ross AB. Reactivity of HO_2/O_2- radicals in aqueous solution. *J Phys Chem Ref Data* 14: 1041–1100, 1985.
6. Bonizzi G, Piette J, Schoonbroodt S, Greimers R, Havard L, Merville MP, and Bours V. Reactive oxygen intermediate-dependent NF-kappaB activation by interleukin-1beta requires 5-lipoxygenase or NADPH oxidase activity. *Mol Cell Biol* 19: 1950–1960, 1999.
7. Cataldo AM, Barnett JL, Pieroni C, and Nixon RA. Increased neuronal endocytosis and protease delivery to early endosomes in sporadic Alzheimer's disease: neuropathologic evidence for a mechanism of increased beta-amyloidogenesis. *J Neurosci* 17: 6142–6151, 1997.
8. Cataldo AM, Mathews PM, Boiteau AB, Hassinger LC, Peterhoff CM, Jiang Y, Mullaney K, Neve RL, Gruenberg J, and Nixon RA. Down syndrome fibroblast model of Alzheimer-related endosome pathology: accelerated endocytosis promotes late endocytic defects. *Am J Pathol* 173: 370–384, 2008.
9. Chaudhuri A, Orme S, Vo T, Wang W, and Cherayil BJ. Phosphorylation of TRAF2 inhibits binding to the CD40 cytoplasmic domain. *Biochem Biophys Res Commun* 256: 620–625, 1999.

10. Chung JY, Lu M, Yin Q, and Wu H. Structural revelations of TRAF2 function in TNF receptor signaling pathway. *Adv Exp Med Biol* 597: 93–113, 2007.
11. Demaurex N and Petheo GL. Electron and proton transport by NADPH oxidases. *Phil Trans R Soc Lond B Biol Sci* 360: 2315–2325, 2005.
12. Deshpande SS, Angkeow P, Huang J, Ozaki M, and Irani K. Rac1 inhibits TNF-alpha-induced endothelial cell apoptosis: dual regulation by reactive oxygen species. *FASEB J* 14: 1705–1714, 2000.
13. Duan D, Li Q, Kao AW, Yue Y, Pessin JE, and Engelhardt JF. Dynamin is required for recombinant adeno-associated virus type 2 infection. *J Virol* 73: 10371–10376, 1999.
14. Fotin-Mleczek M, Welte S, Mader O, Duchardt F, Fischer R, Hufnagel H, Scheurich P, and Brock R. Cationic cell-penetrating peptides interfere with TNF signalling by induction of TNF receptor internalization. *J Cell Sci* 118: 3339–3351, 2005.
15. Frey RS, Rahman A, Kefer JC, Minshall RD, and Malik AB. PKCzeta regulates TNF-alpha-induced activation of NADPH oxidase in endothelial cells. *Circ Res* 90: 1012–1019, 2002.
16. Ganley IG, Carroll K, Bittova L, and Pfeffer S. Rab9 GTPase regulates late endosome size and requires effector interaction for its stability. *Mol Biol Cell* 15: 5420–5430, 2004.
17. Ghosh S and Karin M. Missing pieces in the NF-kappaB puzzle. *Cell* 109(suppl): S81–S96, 2002.
18. Hanna IR, Taniyama Y, Szocs K, Rocic P, and Griendling KK. NAD(P)H oxidase-derived reactive oxygen species as mediators of angiotensin ii signaling. *Antioxid Redox Signal* 4: 899–914, 2002.
19. Harraz MM, Marden JJ, Zhou W, Zhang Y, Williams A, Sharov VS, Nelson K, Luo M, Paulson H, Schoneich C, and Engelhardt JF. SOD1 mutations disrupt redox-sensitive Rac regulation of NADPH oxidase in a familial ALS model. *J Clin Invest* 118: 659–670, 2008.
20. Haxhinasto SA and Bishop GA. Synergistic B cell activation by CD40 and the B cell antigen receptor: role of B lymphocyte antigen receptor-mediated kinase activation and tumor necrosis factor receptor-associated factor regulation. *J Biol Chem* 279: 2575–2582, 2004.
21. Hayden MR and Tyagi SC. Islet redox stress: the manifold toxicities of insulin resistance, metabolic syndrome and amylin derived islet amyloid in type 2 diabetes mellitus. *JOP* 3: 86–108, 2002.
22. Hsu H, Shu HB, Pan MG, and Goeddel DV. TRADD-TRAF2 and TRADD-FADD interactions define two distinct TNF receptor 1 signal transduction pathways. *Cell* 84: 299–308, 1996.
23. Hsu H, Xiong J, and Goeddel DV. The TNF receptor 1-associated protein TRADD signals cell death and NF-kappa B activation. *Cell* 81: 495–504, 1995.
24. Hsu HY and Wen MH. Lipopolysaccharide-mediated reactive oxygen species and signal transduction in the regulation of interleukin-1 gene expression. *J Biol Chem* 277: 22131–22139, 2002.
25. Hu HM, O'Rourke K, Boguski MS, and Dixit VM. A novel RING finger protein interacts with the cytoplasmic domain of CD40. *J Biol Chem* 269: 30069–30072, 1994.
26. Jiang Q, Griffin DA, Barofsky DF, and Hurst JK. Intraphagosomal chlorination dynamics and yields determined using unique fluorescent bacterial mimics. *Chem Res Toxicol* 10: 1080–1089, 1997.
27. Kim YS, Morgan MJ, Choksi S, and Liu ZG. TNF-induced activation of the Nox1 NADPH oxidase and its role in the induction of necrotic cell death. *Mol Cell* 26: 675–687, 2007.
28. Lam SK, Tse YC, Robinson DG, and Jiang L. Tracking down the elusive early endosome. *Trends Plant Sci* 12: 497–505, 2007.
29. Lambeth JD, Kawahara T, and Diebold B. Regulation of Nox and Duox enzymatic activity and expression. *Free Radic Biol Med* 43: 319–331, 2007.
30. Li H and Lin X. Positive and negative signaling components involved in TNFalpha-induced NF-kappaB activation. *Cytokine* 41: 1–8, 2008.
31. Li JM, Mullen AM, Yun S, Wientjes F, Brouns GY, Thrasher AJ, and Shah AM. Essential role of the NADPH oxidase subunit p47(phox) in endothelial cell superoxide production in response to phorbol ester and tumor necrosis factor-alpha. *Circ Res* 90: 143–150, 2002.
32. Li Q, Harraz MM, Zhou W, Zhang LN, Ding W, Zhang Y, Eggleston T, Yeaman C, Banfi B, and Engelhardt JF. Nox2 and Rac1 regulate H2O2-dependent recruitment of TRAF6 to endosomal interleukin-1 receptor complexes. *Mol Cell Biol* 26: 140–154, 2006.
33. Li Q, Sanlioglu S, Li S, Ritchie T, Oberley L, and Engelhardt JF. GPx-1 gene delivery modulates NFkappaB activation following diverse environmental injuries through a specific subunit of the IKK complex. *Antioxid Redox Signal* 3: 415–432, 2001.
34. Li S, Wang L, Berman MA, Zhang Y, and Dorf ME. RNAi screen in mouse astrocytes identifies phosphatases that regulate NF-kappaB signaling. *Mol Cell* 24: 497–509, 2006.
35. Li Y, Zhu H, Kuppusamy P, Roubaud V, Zweier JL, and Trush MA. Validation of lucigenin (*bis-N*-methylacridinium) as a chemilumigenic probe for detecting superoxide anion radical production by enzymatic and cellular systems. *J Biol Chem* 273: 2015–2023, 1998.
36. Liu ZG. Molecular mechanism of TNF signaling and beyond. *Cell Res* 15: 24–27, 2005.
37. Mahadev K, Motoshima H, Wu X, Ruddy JM, Arnold RS, Cheng G, Lambeth JD, and Goldstein BJ. The NAD(P)H oxidase homolog Nox4 modulates insulin-stimulated generation of H2O2 and plays an integral role in insulin signal transduction. *Mol Cell Biol* 24: 1844–1854, 2004.
38. McDermott MF. TNF and TNFR biology in health and disease. *Cell Mol Biol (Noisy-le-grand)* 47: 619–635, 2001.
39. Meier B, Radeke HH, Selle S, Younes M, Sies H, Resch K, and Habermehl GG. Human fibroblasts release reactive oxygen species in response to interleukin-1 or tumour necrosis factor-alpha. *Biochem J* 263: 539–545, 1989.
40. Micheau O and Tschopp J. Induction of TNF receptor I-mediated apoptosis via two sequential signaling complexes. *Cell* 114: 181–190, 2003.
41. Miller FJ Jr, Filali M, Huss GJ, Stanic B, Chamseddine A, Barna TJ, and Lamb FS. Cytokine activation of nuclear factor kappa B in vascular smooth muscle cells requires signaling endosomes containing Nox1 and ClC-3. *Circ Res* 101: 663–671, 2007.
42. Mumbengegwi DR, Li Q, Li C, Bear CE, and Engelhardt JF. Evidence for a superoxide permeability pathway in endosomal membranes. *Mol Cell Biol* 28: 3700–3712, 2008.
43. Murk JL, Posthuma G, Koster AJ, Geuze HJ, Verkleij AJ, Kleijmeer MJ, and Humbel BM. Influence of aldehyde fixation on the morphology of endosomes and lysosomes: quantitative analysis and electron tomography. *J Microsc* 212: 81–90, 2003.
44. Natoli G, Costanzo A, Ianni A, Templeton DJ, Woodgett JR, Balsano C, and Levrero M. Activation of SAPK/JNK by TNF receptor 1 through a noncytotoxic TRAF2-dependent pathway. *Science* 275: 200–203, 1997.

45. Nishitoh H, Saitoh M, Mochida Y, Takeda K, Nakano H, Rothe M, Miyazono K, and Ichijo H. ASK1 is essential for JNK/SAPK activation by TRAF2. *Mol Cell* 2: 389–395, 1998.
46. Oakley FD, Abbott D, Li Q, and Engelhardt JF. Signaling components of redox active endosomes: the redoxosomes. *Antioxid Redox Signal* (this issue).
47. Pagano PJ, Clark JK, Cifuentes-Pagano ME, Clark SM, Callis GM, and Quinn MT. Localization of a constitutively active, phagocyte-like NADPH oxidase in rabbit aortic adventitia: enhancement by angiotensin II. *Proc Natl Acad Sci USA* 94: 14483–14488, 1997.
48. Pollock JD, Williams DA, Gifford MA, Li LL, Du X, Fisherman J, Orkin SH, Doerschuk CM, and Dinauer MC. Mouse model of X-linked chronic granulomatous disease, an inherited defect in phagocyte superoxide production. *Nat Genet* 9: 202–209, 1995.
49. Rhee SG, Bae YS, Lee SR, and Kwon J. Hydrogen peroxide: a key messenger that modulates protein phosphorylation through cysteine oxidation. *Sci STKE* 2000: PE1, 2000.
50. Rothe M, Wong SC, Henzel WJ, and Goeddel DV. A novel family of putative signal transducers associated with the cytoplasmic domain of the 75 kDa tumor necrosis factor receptor. *Cell* 78: 681–692, 1994.
51. Sanlioglu S, Williams CM, Samavati L, Butler NS, Wang G, McCray PB Jr, Ritchie TC, Hunninghake GW, Zandi E, and Engelhardt JF. Lipopolysaccharide induces Rac1-dependent reactive oxygen species formation and coordinates tumor necrosis factor-alpha secretion through IKK regulation of NF-kappa B. *J Biol Chem* 276: 30188–30198, 2001.
52. Segal AW and Coade SB. Kinetics of oxygen consumption by phagocytosing human neutrophils. *Biochem Biophys Res Commun* 84: 611–617, 1978.
53. Sheikh MS and Huang Y. Death receptor activation complexes: it takes two to activate TNF receptor 1. *Cell Cycle* 2: 550–552, 2003.
54. Shen HM, Lin Y, Choksi S, Tran J, Jin T, Chang L, Karin M, Zhang J, and Liu ZG. Essential roles of receptor-interacting protein and TRAF2 in oxidative stress-induced cell death. *Mol Cell Biol* 24: 5914–5922, 2004.
55. Souza HP, Liu X, Samouilov A, Kuppusamy P, Laurindo FR, and Zweier JL. Quantitation of superoxide generation and substrate utilization by vascular NAD(P)H oxidase. *Am J Physiol Heart Circ Physiol* 282: H466–H474, 2002.
56. Sundaresan M, Yu ZX, Ferrans VJ, Irani K, and Finkel T. Requirement for generation of H2O2 for platelet-derived growth factor signal transduction. *Science* 270: 296–299, 1995.
57. Tartaglia LA and Goeddel DV. Two TNF receptors. *Immunol Today* 13: 151–153, 1992.
58. Trischler M, Stoorvogel W, and Ullrich O. Biochemical analysis of distinct Rab5- and Rab11-positive endosomes along the transferrin pathway. *J Cell Sci* 112: 4773–4783, 1999.
59. Ushio-Fukai M. Localizing NADPH oxidase-derived ROS. *Sci STKE* 2006: re8, 2006.
60. Venkataraman S, Martin SM, Schafer FQ, and Buettner GR. Detailed methods for the quantification of nitric oxide in aqueous solutions using either an oxygen monitor or EPR. *Free Radic Biol Med* 29: 580–585, 2000.
61. Winterbourn CC, Hampton MB, Livesey JH, and Kettle AJ. Modeling the reactions of superoxide and myeloperoxidase in the neutrophil phagosome: implications for microbial killing. *J Biol Chem* 281: 39860–39869, 2006.
62. Yoshizumi M, Tsuchiya K, and Tamaki T. Signal transduction of reactive oxygen species and mitogen-activated protein kinases in cardiovascular disease. *J Med Invest* 48: 11–24, 2001.

Address reprint requests to:
John F. Engelhardt, Ph.D.
Room 1-111 BSB
Department of Anatomy and Cell Biology
College of Medicine, University of Iowa
51 Newton Road
Iowa City, IA 52242

E-mail: john-engelhardt@uiowa.edu

Date of first submission, December 15, 2008; date of acceptance, December 29, 2008.

This article has been cited by:

1. Michael J. Surace, Michelle L. Block. 2012. Targeting microglia-mediated neurotoxicity: the potential of NOX2 inhibitors. *Cellular and Molecular Life Sciences* **69**:14, 2409-2427. [CrossRef]
2. Yonggang Zhang, Wenhui Hu. 2012. NF#B signaling regulates embryonic and adult neurogenesis. *Frontiers in Biology* . [CrossRef]
3. O. F. Araneda, M. Tuesta. 2012. Lung Oxidative Damage by Hypoxia. *Oxidative Medicine and Cellular Longevity* **2012**, 1-18. [CrossRef]
4. S Song, K Choi, S-W Ryu, S W Kang, C Choi. 2011. TRAIL promotes caspase-dependent pro-inflammatory responses via PKC# activation by vascular smooth muscle cells. *Cell Death and Disease* **2**:11, e223. [CrossRef]
5. Javier Escobar, Javier Pereda, Gerardo López-Rodas, Juan Sastre. 2011. Redox signaling and histone acetylation in acute pancreatitis. *Free Radical Biology and Medicine* . [CrossRef]
6. Hai Chen, Gab Seok Kim, Nobuya Okami, Purnima Narasimhan, Pak H. Chan. 2011. NADPH oxidase is involved in post-ischemic brain inflammation. *Neurobiology of Disease* **42**:3, 341-348. [CrossRef]
7. Michael J. Morgan, Zheng-gang Liu. 2010. Reactive oxygen species in TNF#-induced signaling and cell death. *Molecules and Cells* **30**:1, 1-12. [CrossRef]
8. Hye-Lim Lee, Kyung Mi Woo, Hyun-Mo Ryoo, Jeong-Hwa Baek. 2010. Tumor necrosis factor-# increases alkaline phosphatase expression in vascular smooth muscle cells via MSX2 induction. *Biochemical and Biophysical Research Communications* **391**:1, 1087-1092. [CrossRef]
9. David I. Brown, Kathy K. Griendling. 2009. Nox proteins in signal transduction. *Free Radical Biology and Medicine* **47**:9, 1239-1253. [CrossRef]
10. Barrie J. Carter , Pervin Anklesaria , Stephanie Choi , John F. Engelhardt . 2009. Redox Modifier Genes and Pathways in Amyotrophic Lateral Sclerosis. *Antioxidants & Redox Signaling* **11**:7, 1569-1586. [Abstract] [Full Text PDF] [Full Text PDF with Links]
11. Fred S. Lamb , Jessica G. Moreland , Francis J. Miller Jr. . 2009. Electrophysiology of Reactive Oxygen Production in Signaling Endosomes. *Antioxidants & Redox Signaling* **11**:6, 1335-1347. [Abstract] [Full Text PDF] [Full Text PDF with Links]